

# What can cosmic-ray knees reveal about source populations?

Myrto Falalaki<sup>1,2</sup> and Vasiliki Pavlidou<sup>1,2</sup>

<sup>1</sup> University of Crete, Department of Physics & Institute of Theoretical & Computational Physics, 70013 Herakleio, Greece  
e-mail: ph5690@edu.physics.uoc.gr; pavlidou@physics.uoc.gr

<sup>2</sup> Institute of Astrophysics, Foundation for Research and Technology-Hellas, 71110 Heraklion, Crete, Greece

Received / accepted

## ABSTRACT

**Context.** Breaks in the cosmic ray (CR) flux spectrum encode information on the properties of CR accelerator populations producing the observed flux. Spectral steepenings, known as knees, are generally accompanied by a transition to heavier composition.

**Aims.** We seek generic features of CR source populations that imprint onto knee observables in a manner that is robust enough and distinct enough to be discernible even in the presence of significant uncertainties and systematics in CR data. In particular, we explore how diversity among population members could imprint on the knee phenomenology, under the assumption that a knee is due to a fixed-rigidity cutoff in the source spectrum.

**Methods.** We use a simple theoretical model for a population of CR accelerators. Each member of the population accelerates CR stochastically to a power-law spectrum, up to a cutoff rigidity, resulting from source-confinement requirements. We allow for variance among members, in the cutoff rigidity and in the power-law slope.

**Results.** We find that: (a) the slope step of the flux spectrum is  $\sim 0.5$ , decreasing weakly with increasing spread in either property; (b) composition always breaks first; (c) the difference between the break energies in composition and flux increases with increasing diversity; (d) composition and flux break together only if population diversity is minimal. These trends are robust under our assumptions; deviations from them in observed data would indicate more complex physics than encoded in our simple model.

**Conclusions.** Comparing these trends with observed CR knees, we conclude that: (i) the primary knee at  $\sim 4 \times 10^{15}$  eV is consistent with a constant-rigidity cutoff according to KASCADE-Grande data processed with post-LHC hadronic models, but not according to other datasets; (ii) the second knee at  $\sim 5 \times 10^{17}$  eV conclusively requires more complexity than the cutoff of a single CR source population; (iii) the spectral feature identified by Auger at  $\sim 10^{19}$  eV is consistent with a constant-rigidity source cutoff only if there is a substantial spread in both cutoff rigidity and slope in the parent source population. Interestingly, a significant spread in slope would also result in spectral curvature before the break, which would in turn be contributing to the ankle feature.

**Key words.** cosmic rays, energy spectrum, knee, composition, Methods: statistical

## 1. Introduction

The energy spectrum of cosmic radiation is a critical observable for our understanding of the nature of cosmic ray (CR) accelerators. This spectrum can be described as a power law over many orders of magnitude (from  $\sim 10^9$  eV to  $\sim 10^{20}$  eV). The spectral power index, however, exhibits changes at characteristic energies, referred to as knees (when the spectrum steepens) and ankles (when the spectrum flattens).

Knees have now been spectrally resolved in great detail at several different energies in the CR spectrum, ranging from few times  $10^{15}$  eV to  $10^{19}$  eV (e.g., Nagano et al. 1984; Cassiday et al. 1990; Fowler et al. 2001; Hires/Mia Collaboration 2001; Antoni et al. 2005; Abbasi et al. 2005; Amenomori et al. 2008; Aartsen et al. 2013; Aab et al. 2020; Cao et al. 2024). These breaks are typically accompanied by transitions to heavier composition around the same energies as the spectral break (e.g., Chiavassa et al. 2019; Aab et al. 2020). This behavior has led to the qualitative interpretation of the knee phenomenon as a constant-rigidity cutoff (also referred to as Peters cycle, Peters 1961), either in Galactic confinement or in source acceleration / confinement: particles accelerated stochastically by a CR source cannot reach energies beyond the threshold where magnetic confinement is lost. This effect occurs roughly at the energy where a particle's gyroradius in the source's magnetic field becomes comparable to the size of the source (e.g., Hillas 1984).

A rich literature exists on quantitative models of the various knee-like breaks of the CR spectrum, ranging from fits of specific datasets with complex phenomenological models, to comprehensive physical models, including specific hypotheses on source accelerator physics and source population properties, propagation effects, and simulations of atmospheric air showers to obtain direct observables (e.g., Hillas 1979; Sveshnikova 2003; Hörandel 2004; Lemoine 2005; Kotera & Lemoine 2008; Bijay & Bhadra 2016; Aab et al. 2017; Kimura et al. 2018; Mollerach & Roulet 2019; Guido et al. 2022; Mukhopadhyay et al. 2023; Muzio et al. 2024).

Despite these intensive theoretical and experimental efforts, the exact characteristics, nature and origin of *all* observed CR knees is still under debate. One very important factor contributing to this continued uncertainty is that the data are not yet fully converged. High-level observables (i.e. spectra and moments of the log mass-number distribution) can differ between observatories using different observational techniques at the same energies (see e.g. review of data on the primary knee in Blümer et al. 2009); between different observatories using similar techniques (see, e.g., differences in flux and composition at the highest energies reported by the Pierre Auger Observatory and Telescope Array, Deligny 2020; Yushkov et al. 2019); between events recorded by the same observatory when using different observables (see, e.g., differences in composition at ultra-

high energies derived when using shower depth or shower muon content, e.g., [Sanchez-Lucas 2017](#)); and even between identical recorded datasets when processed with different simulations of hadronic interactions (for example, with pre- versus post-LHC models, [Antoni et al. 2005](#); [Chiavassa et al. 2019](#); or with different hadronic interaction packages of the same generation, [Yushkov 2019a](#)). As a result, detailed fits to sophisticated source population models may fail or return parameters that appear astrophysically contrived (e.g., [Aab et al. 2017](#); [Ehlert et al. 2023](#)), not because the models are necessarily inconsistent with the actual source populations, but rather because our data from said source populations might be affected by systematics that are not adequately quantified or accounted for.

The question then arises whether there exist any generic features of cosmic-ray source populations that imprint onto cosmic-ray observables in a manner that is robust enough and distinct enough to be discernible even in such a still-fluid experimental landscape. This is our aim in this paper. Using the simplest possible model for an underlying population of CR accelerators, we seek to build insight on how the diversity between population members could imprint on the knee phenomenology, under the assumption that a knee is a fixed-rigidity-cutoff phenomenon. Such insight is necessary in order to identify any robust features and trends of simple population models and their most straightforward variations. Absence of said features would then constitute evidence of more complex physics of either CR acceleration (complicated astrophysics) or CR interactions at the detection site (unexpected particle physics).

A knee is described phenomenologically by the characteristic energy where the break occurs in the CR flux spectrum, by the spectral slopes before and after this characteristic energy, and the (generally different) energy where the accompanying break in CR composition takes place. We will investigate whether features of the population of CR sources responsible for the knee result in patterns in these observables that are simple and robust enough that they might be recognizable even in the presence of significant systematic uncertainties in the data.

To this end, we set up a simple, generic model for a population of CR accelerators with the following properties: (a) For energies well below its rigidity cutoff (equal to the proton cutoff energy,  $E_{p,\max}$ ), each source contributes to the Galactic CR flux particles with a power-law spectrum of energies of slope  $\gamma$  (encoding both the source acceleration properties, and losses during propagation). (b) The rigidity cutoff can be described by an exponential suppression of the power-law spectrum. Different nuclei cutoff at different energies scaling as  $ZE_{p,\max}$ . (c) We allow diversity between members of the CR source population in both  $E_{p,\max}$  and  $\gamma$ . A "knee" observed in the summed CR spectrum due to such a population of sources will consist of: a break in the spectrum, encoding, but not necessarily equal to,  $E_{p,\max}$ ; and a break in the composition at a similar, but not necessarily identical, energy. The location in energy of those breaks, and the slope difference between and after the knee will be modulated by the distribution of  $\gamma$  and  $E_{p,\max}$  among the individual members of the population.

We explore the features and trends of this simple model, and in particular we address the following specific questions: (1) Under what conditions do the flux spectrum and composition spectrum break together? (2) When they do not, which one breaks first? (3) How do the break energies relate to  $E_{p,\max}$ ? (4) How does the diversity of the population properties, manifesting as a spread in  $E_{p,\max}$  and  $\gamma$ , affect the answers to these questions?

This paper is organized as follows. In §2 we lay out the formulation of our model, emphasizing its free parameters and their

impact on the observable flux and composition spectra. In §3 we explore the behavior of these observables as the population diversity increases. We summarize our conclusions and discuss them in the context of observations of various CR knees in §4.

## 2. The model

### 2.1. Single Source

We implement a fixed-rigidity cutoff, characteristic of CR sources relying on magnetic confinement ([Hillas 1984](#); [Hörandel 2004](#)). We do so by assuming that the differential flux  $F_z$  produced by a single cosmic ray source as a function of the energy  $E$  of primary particles of charge  $Z$  has the form:

$$F_z(E) = F_0(Z) \left( \frac{E}{E_0} \right)^{-\gamma} \exp \left[ -\frac{E}{ZE_{p,\max}} \right] \quad (1)$$

where  $E_{p,\max}$  is the rigidity cutoff,  $F_0(Z)$  is the flux of a specific species of atomic number  $Z$  at some normalization energy  $E_0 \ll E_{p,\max}$ , and  $\gamma$  is the low-energy power-law slope. In our model, we assume that  $\gamma$  is identical for all species in a single source, and that it encodes both acceleration and propagation physics (including losses and escape).

The total flux from a single source at an energy  $E$  will be the sum of  $F_z(E)$  over all primary charges:

$$F(E) = \sum_Z F_z(E). \quad (2)$$

In this work, we have taken the relative abundances  $F_0(Z)$  from [Zhao et al. \(2015\)](#) (see their table 1, where they present their fitted parameters for a power-law like model for every nuclei). While [Zhao et al. \(2015\)](#) fit a different slope  $\gamma_z$  for different species, we have adopted here an effective value of  $\gamma \approx 2.66$  for all species. However, our results are independent of the exact choice for the value of  $\gamma$ , since we always plot deviations (differences) of fitted slopes from the underlying source  $\gamma$ . We simulate fluxes for the following individual species: H, He, C, O, Ne, Mg, Si and Fe. These abundances are observationally motivated for energies below the primary CR knee; however our qualitative conclusions do not depend sensitively on this choice, and so they hold for any source population accelerating particles of mixed composition roughly comparable to that of Galactic CR, even if the pre-break abundances differ in their details from the ones we have adopted here.

We quantify the resulting composition spectrum by the average of the logarithm of the mass number as a function of energy,  $\langle \ln A \rangle(E)$ , since this metric is frequently used to summarize CR composition observations. For a single source, this will be given by

$$\langle \ln A \rangle(E) = \frac{\sum_Z F_z(E) \ln(A_z)}{\sum_Z F_z(E)}. \quad (3)$$

### 2.2. Source population

The CR observables on Earth at a given energy are produced by particles accelerated by a population of sources with a distribution of sizes, B-fields and other properties. Variations in these physical conditions among population members will result in corresponding variations of source model parameters (see, e.g., [Workman et al. 2022](#); [Diesing 2023](#)). In our simple source model, these parameters are  $F_0(Z)$ ,  $\gamma$ , and  $E_{p,\max}$ . In this work, we are interested in any signatures of the diversity in  $E_{p,\max}$  and

$\gamma$  imprinted on the observables of a knee produced by a constant-rigidity cutoff in the spectra of sources. To isolate the effects of each of these source properties, we explore the effect of increasing spread in one of  $E_{p,\max}$ ,  $\gamma$ , while keeping the distribution of the other fixed to a delta function. We also make the simplifying assumption that relative values of  $\tilde{f}_0(Z) = F_0(Z)/F_0(Z=1)$  (the accelerated particles relative abundances at energies well below the proton cutoff) are identical among different population members, so that the only quantities that may vary between individual CR sources are  $F_0(Z=1)$ ,  $E_{p,\max}$ , and  $\gamma$ .

Mathematically, we model this picture as follows. Choosing a normalization energy  $E_0$  well below the lowest  $E_{p,\max}$  encountered in the specific population, the exponential suppression factor in Eq. (1) at  $E_0$  is equal to 1 for all sources. The resulting total flux from all population sources at that energy can be calculated as:

$$F_{Z,\text{tot}}(E_0 \ll \min E_{p,\max}) = \sum_i F_{0,i}(Z=1)\tilde{f}_0(Z) \equiv F_{Z,\text{tot},0}, \quad (4)$$

where the summation is over different population member sources. This equation defines the flux normalization of species  $Z$  for the population,  $F_{Z,\text{tot},0}$ .

To calculate the spectrum at higher energies, we introduce the probability distributions  $p_E(E_{p,\max})$  and  $p_\gamma(\gamma)$  of the cutoff rigidity, and the low-energy power-law slope, respectively, in the population. Formally,  $p_E(E_{p,\max})dE_{p,\max}$  is the fraction of particles at energy  $E_0$  that were accelerated by sources with rigidity cutoffs between  $E_{p,\max}$  and  $E_{p,\max} + dE_{p,\max}$ ; and  $p_\gamma(\gamma)d\gamma$  is the fraction of particles accelerated by sources that, had they been responsible for the entire CR spectrum at low energies, would have produced (after acceleration and propagation) a spectrum which would have been a superposition of power laws with slopes between  $\gamma$  and  $\gamma + d\gamma$ . Then, the total flux of species  $Z$  due to the entire population can be calculated through

$$F_{Z,\text{tot}}(E) = F_{Z,\text{tot},0} \int_0^\infty dE_{p,\max} p_E(E_{p,\max}) e^{-\frac{E}{ZE_{p,\max}}} \int_0^\infty d\gamma p_\gamma(\gamma) \left(\frac{E}{E_0}\right)^{-\gamma}. \quad (5)$$

The total CR flux due to all species will be

$$F_{\text{tot}}(E) = \sum_Z F_{z,\text{tot}}(E). \quad (6)$$

Finally, the composition spectrum due to the population will be given by

$$\langle \ln A \rangle_{\text{tot}}(E) = \frac{\sum_Z F_{Z,\text{tot}}(E) \ln(A_Z)}{\sum_Z F_{Z,\text{tot}}(E)}. \quad (7)$$

### 2.3. Varying $E_{p,\max}$

We will estimate the effect of a spread in  $E_{p,\max}$  among population members by assuming  $p_E(E_{p,\max})$  is lognormal:

$$p_E(E_{p,\max}) = \frac{1}{E_{p,\max} \sigma \sqrt{2\pi}} \exp\left[-\frac{(\ln E_{p,\max} - \mu)^2}{2\sigma^2}\right]. \quad (8)$$

The parameters of the distribution  $\mu$  and  $\sigma$  are related to the mean and the standard deviation of the distribution through

$$\mu = \ln\left(\frac{\bar{E}_{p,\max}^2}{\sqrt{\bar{E}_{p,\max}^2 + \sigma_{E_{p,\max}}^2}}\right) \quad (9)$$

and

$$\sigma^2 = \ln\left[1 + \left(\frac{\sigma_{E_{p,\max}}}{\bar{E}_{p,\max}}\right)^2\right]. \quad (10)$$

The advantage of the lognormal distribution is that  $E_{p,\max}$  is positive definite and as a result arbitrarily large values of  $\sigma_{E_{p,\max}}$  can be accommodated, allowing us to examine asymptotic behaviors for very diverse populations. The distribution  $p_\gamma$  remains fixed to a delta function.

### 2.4. Varying $\gamma$

To estimate the effect of a spread in  $\gamma$ , we keep  $p_E(E_{p,\max})$  fixed to a delta function, and we implement a Gaussian  $p_\gamma(\gamma)$ , with mean  $\bar{\gamma}$  and spread  $\sigma_\gamma$ . In this case, Eq.(5) has an analytic solution,

$$F_{Z,\text{tot}}(E) = F_{z,\text{tot},0} \exp\left[-\frac{E}{ZE_{p,\max}}\right] \left(\frac{E}{E_0}\right)^{-\bar{\gamma}} \exp\left[-\frac{\sigma_\gamma^2}{2} \ln^2\left(\frac{E}{E_0}\right)\right]. \quad (11)$$

### 2.5. Observables

Even though the flux suppression of individual CR species is exponential, the fact that the suppression sets in at increasing energy for increasing  $Z$  results to a flattening of the knee. This will be true for individual sources (Eq. 2), and more so for a population (Eq. 6) where the spread in  $E_{p,\max}$  and/or  $\gamma$  will result in a smoother break. Observed knees can be fitted well by broken power laws, and we attempt the same for our model results. In particular, we test whether a broken power law of the form:

$$F_{\text{tot}}(E) = C \times \begin{cases} \left(\frac{E}{E_b}\right)^{-\gamma_1}, & E \leq E_b \\ \left(\frac{E}{E_b}\right)^{-\gamma_2}, & E > E_b \end{cases} \quad (12)$$

can describe adequately the total flux around the knee. From this fit, we extract "observables"  $\gamma_1$  (slope before the break),  $\gamma_2$  (slope after the break), and  $E_b$  (break energy).

We additionally evaluate a fourth "observable", the composition break energy,  $E_A$ . We do so by: (a) fitting the composition spectrum of Eq. (7) for  $E \ll \bar{E}_{p,\max}$  by a constant (horizontal line); and (b) fitting the composition spectrum by a logarithmic increase (linear increase with  $\log E$ ) for  $E \gg \bar{E}_{p,\max}$ . Then,  $E_A$  is the energy at which the two lines intersect (see lower-right panel of Fig. 1).

## 3. Results

We start by examining the trends induced on the "observables" by a gradually increasing spread in  $E_{p,\max}$  among population members.

In the upper left panel of Fig. 1 we show the all-particle spectrum (flattened by  $E^\gamma$ ) as we evaluate it from Eqs. (5) and (6) and for a lognormal  $p(E_{p,\max})$ , for  $\sigma_{E_{p,\max}} \in [0, 3\bar{E}_{p,\max}]$ . For broader  $p(E_{p,\max})$ , the all-particle spectrum deviates sooner (at lower energies) from its low-energy asymptotic behavior, as a result of the property of the lognormal distribution to peak around values of  $E_{p,\max} < \bar{E}_{p,\max}$ . At the same time, the spectrum falls less steeply at high energies, owing to the tail of the longnormal towards high  $E_{p,\max}$  values.

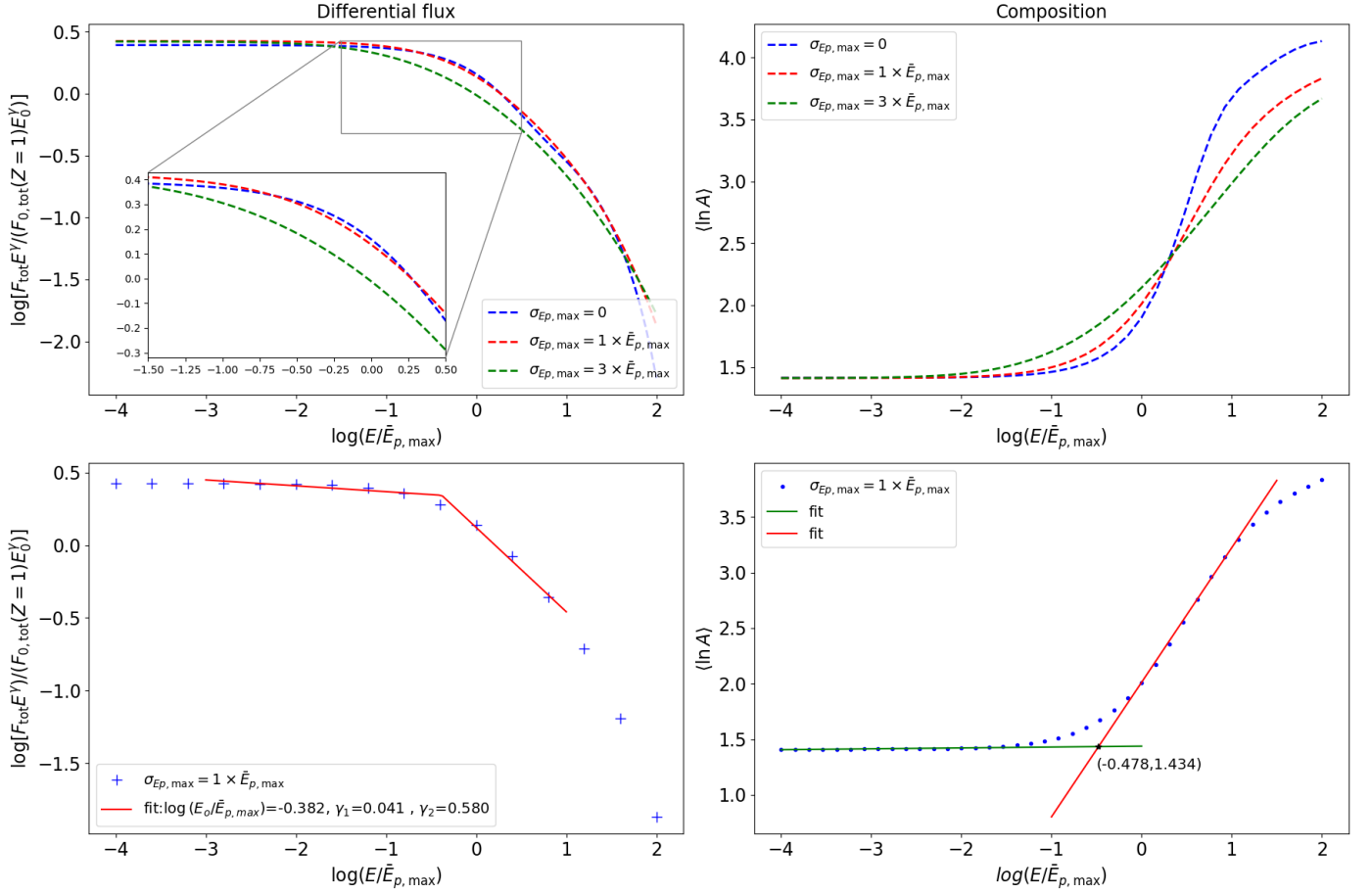


**Fig. 1.** All-particle flux and composition spectra in the case of a lognormal  $p(E_{p,\max})$ . Upper-left panel: all particle flux spectrum flattened by  $E^\gamma$ . Upper-right panel: composition spectrum. Lower-left panel: broken power-law fit around the knee for the flux spectrum. Crosses correspond to mock observations obtained from our model. The solid line is the fit of Eq. (12). Lower-right panel: low- and high-energy asymptotic logarithmic fits to the composition spectrum (green and red solid lines respectively). Points again correspond to mock data obtained from our model. The composition break energy given by the intersection of the two lines (black star).

In the lower-left panel of Fig. 1, we show an example of fitting the all-particle flux spectrum around the knee with a broken power law. The case depicted here is produced by setting  $\sigma_{E_{p,\max}} = E_{p,\max}$  in the lognormal  $p(E_{p,\max})$ . It is through such fits that we obtain the break point  $E_b$  and the spectral power indices  $\gamma_1, \gamma_2$  (the "observables" discussed in the context of Eq. 12), which we present and discuss in Figs. 2 and 3 as functions of  $\sigma_{E_{p,\max}}$ .

The upper-right panel of Fig. 1 shows the composition spectrum for the same models as in the upper-left panel. The break in flux is accompanied by a break in composition. The impact of increasing  $\sigma_{E_{p,\max}}$  on the composition spectrum is more pronounced than that on the flux spectrum, both towards lower and higher energies, as well as in terms of the steepness of the break. To quantify this behavior, we again fit the low-energy and high-energy trends with logarithmic functions ( $\langle \ln A \rangle$  linear in  $\log E$ ), as shown in the lower-right panel of Fig. 1. The intersection of the two fits defines the composition break energy,  $E_A$ .

The effect of  $\sigma_{E_{p,\max}}$  on the "observables" is shown in Figs. 2 and 3. Figure 2 shows the exponents  $\gamma_1$  and  $\gamma_2$  (slopes before and after the break, red and blue points respectively), evaluated as difference from the single-source slope  $\gamma$ . The error budget is completely dominated by systematic uncertainties, primarily driven by the choice of points to include in the fit. Here, error bars correspond to the difference between including or dropping

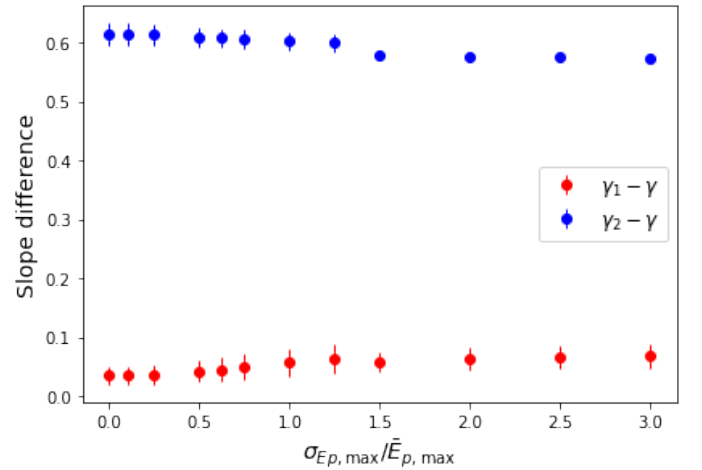


**Fig. 2.** Values of the spectral power indices  $\gamma_1$  and  $\gamma_2$ , indicated with red and blue points respectively, as a function of  $\sigma_{E_{p,\max}}/E_{p,\max}$ .

an extra point at the high-energy tail of the fit (see lower-left panel of Fig. 1).

The difference between the two slopes starts at  $\sim 0.6$  for a population comprised of members with identical  $E_{p,\max}$

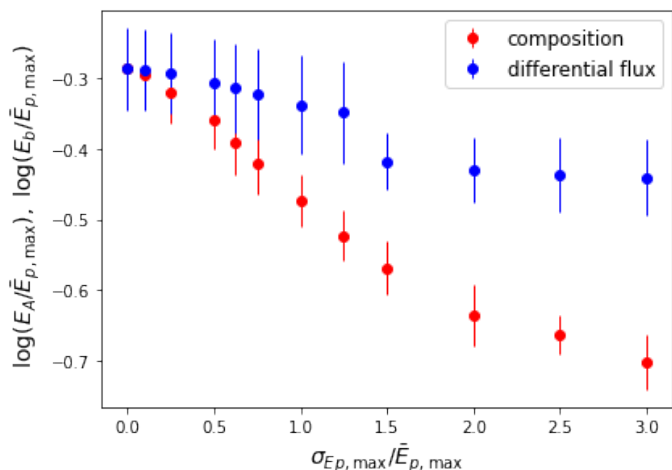


**Fig. 3.** Energies of the composition break (red) and the flux break (blue) in units of  $\bar{E}_{p,\max}$  as a function of  $\sigma_{E_{p,\max}}/\bar{E}_{p,\max}$ .

( $\sigma_{E_{p,\max}} = 0$ ), and decreases slowly as  $\sigma_{E_{p,\max}}$  increases, reaching  $\sim 0.5$  for  $\sigma_{E_{p,\max}} = 3\bar{E}_{p,\max}$ . This mild trend is a result of two compounding effects. First, as  $\sigma_{E_{p,\max}}$  increases, the number of sources with low  $E_{p,\max}$  also increases, so the low-energy branch of the broken power law is also affected (becomes steeper,  $\gamma_1$  increases) as some sources have already started becoming suppressed at low energies. Second, a high  $\sigma_{E_{p,\max}}$  also results in a larger number of sources with high  $E_{p,\max}$ . The flux of these sources is not suppressed until higher energies, resulting in a smoother decline of the all-particle spectrum. The high-energy branch of the power law thus becomes shallower ( $\gamma_2$  decreases). The overall conclusion is that a fixed-rigidity cutoff in a CR source population with identical power-law slopes  $\gamma$  and a pre-break composition roughly comparable to that of Galactic CR produces a knee with a slope change in the range of  $\sim 0.5 - 0.6$ , regardless of spread in  $E_{p,\max}$ .

In Fig. 3 we overplot the break energies of the spectrum ( $E_b$ , blue points) and of the composition ( $E_A$ , red points) as a function of the spread in  $E_{p,\max}$ . Error bars are again dominated by systematics. For  $E_b$ , they are obtained in the same way as the error bars in  $\gamma_1$  and  $\gamma_2$ . In the case of  $E_A$ , they correspond to the difference resulting from retaining or dropping one point towards the break in the rising part of the composition spectrum. We observe that in the case of a population with members of identical, or very similar,  $E_{p,\max}$ , composition and flux spectrum break together, at an energy about half of  $E_{p,\max}$ . As  $\sigma_{E_{p,\max}}$  increases both the composition and the flux spectrum break earlier, however  $E_A$  decreases faster than  $E_b$ , and as a result *composition always breaks first*.

We now turn to trends in "observables" that result from a spread in  $\gamma$  among population members. For these calculations, we keep  $p_E(E_{p,\max})$  fixed to a delta function. In Fig. 4 we plot the all-particle spectrum (flattened by  $E^{\bar{\gamma}}$ ) as we evaluate it from Eqs. (5) and (6) and for a Gaussian  $p_\gamma(\gamma)$ . Different line colors correspond to different values of  $\sigma_\gamma$ . Here, the range of  $\sigma_\gamma$  we consider is much narrower than the range of  $\sigma_{E_{p,\max}}$ . The reason is that a large spread in power law indices results in significant spectral curvature (see e.g. black dashed line in Fig. 4), which is not generally seen in the CR spectrum. Interestingly, small spreads in  $\gamma$  appear to generate diversity in the flux spectrum comparable to that produced by very substantial spreads in  $E_{p,\max}$ .

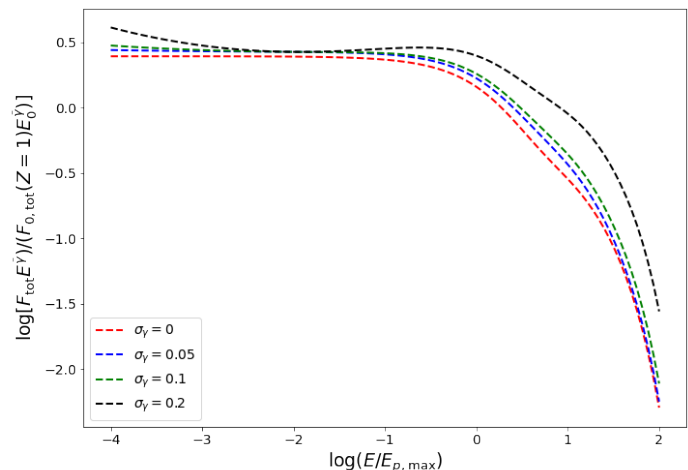


**Fig. 4.** All-particle spectrum flattened by  $E^{\bar{\gamma}}$ , as produced by Eq. (6) with a Gaussian  $p_\gamma(\gamma)$  and a delta-function  $p_E(E_{p,\max})$ . Different lines correspond to different values of  $\sigma_\gamma$ , shown in the legend.

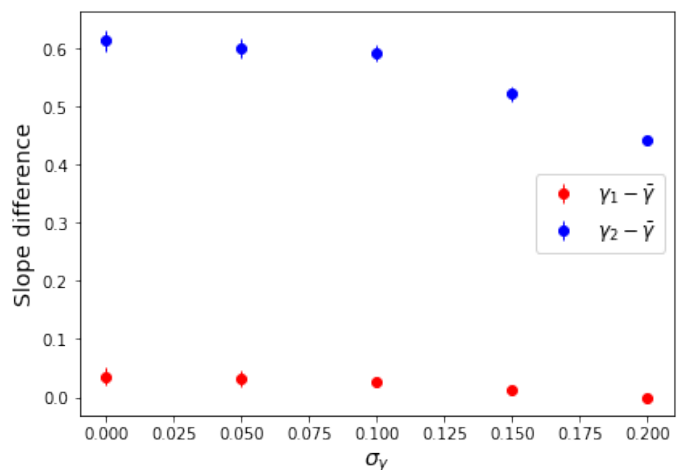


**Fig. 5.** Values of the spectral power indices  $\gamma_1$  and  $\gamma_2$ , indicated with red and blue points respectively, as a function of  $\sigma_\gamma$ .

We investigate the qualitative direction of the trends seen in the "observables" with increasing  $\sigma_\gamma$ , and quantify them, in Figs. 5 and 6. The trend of the sharpness of the break with  $\sigma_\gamma$  is shown in Fig. 5. Colors and error bars are as in Fig. 2. Here again the slope step decreases with increasing population spread, from about 0.6 for a population with no spread, to about 0.45 for  $\sigma_\gamma = 0.2$ , driven primarily by the post-break slope becoming shallower. Still, the effect is very mild: in a standard fixed-rigidity-cutoff knee, the slope change does not become very different from a 0.5 step, even if the underlying accelerator population exhibits significant spread in its properties.

The trends in energy breaks however are now different, as is shown in Fig. 6. The location of the composition break,  $E_A$ , is unaffected by any spread in  $\gamma$ . The flux spectrum break,  $E_b$ , on the other hand *increases* with increasing population spread: the more diverse in  $\gamma$  the population, the later the flux spectrum breaks. Importantly, the overall result goes in the same direction as in the case of a spread in  $E_{p,\max}$ : *composition always breaks first*.

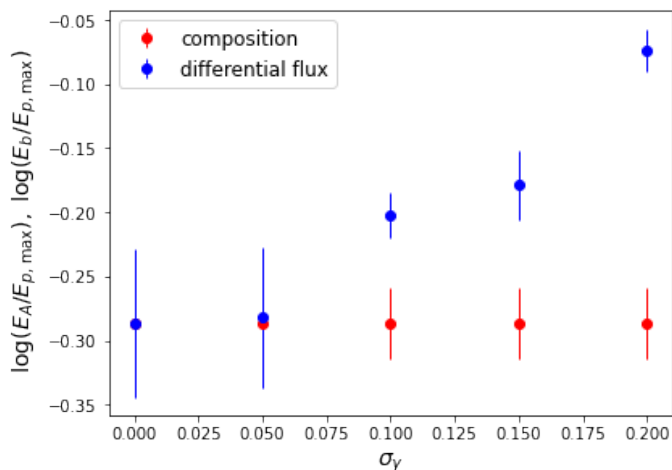


**Fig. 6.** Energies of the composition break (red) and the flux break (in blue) in units of  $E_{p,max}$  as a function of  $\sigma_\gamma$ .

#### 4. Conclusions and Discussion

We have used the simplest possible model of a knee induced by a fixed-rigidity CR-source cutoff, in order to explore how diversity among the members of the underlying cosmic-ray accelerator population affects the knee phenomenology. In particular, we explored how diversity in (a) the rigidity cutoff  $E_{p,max}$  and (b) in the pre-knee cosmic-ray slope  $\gamma$  (encoding both acceleration and loss/propagation physics) is imprinted in (i) the difference in pre- and post-break flux spectrum slopes, and (ii) in the break energies of the flux and composition spectra. We have identified the following robust trends.

1. A knee induced by a fixed-rigidity cutoff in the CR source population exhibits a steep break in the all-particle spectrum, with a slope step around 0.5. Diversity in the population (in either  $E_{p,max}$  or  $\gamma$ ) tends to somewhat reduce the steepness of the break, but the effect is weak.

2. Diversity in  $E_{p,max}$  moves both the flux break energy,  $E_b$ , and the composition break energy,  $E_A$ , to lower values, with the composition being more strongly affected. In contrast, diversity in  $\gamma$  leaves  $E_A$  practically unaffected, but moves  $E_b$  to higher energies.

3. Any diversity in either  $E_{p,max}$  or  $\gamma$  works to separate  $E_b$  from  $E_A$ , in the same direction: *composition breaks first*. The difference between the two can be as large as a factor of several, especially if both  $E_{p,max}$  and  $\gamma$  vary substantially among population members.

4. An observation of the composition and flux breaking around the same energy would constitute an indication of minimal spread in *both*  $E_{p,max}$  and  $\gamma$  in the underlying CR source population.

Any qualitative deviation from these trends would require a model of significantly higher astrophysical complexity than the one we discussed here. Additions to the physics generating the observed flux and composition spectra that could break these trends include, for example, the presence of multiple, distinct populations of cosmic ray accelerators contributing at different flux levels, or intergalactic propagation effects if relevant at the energies under consideration.

We can use these insights to discuss qualitatively the likelihood of each of the steepening features in the broadband cosmic-ray spectrum being a simple fixed-rigidity CR-source-

cutoff knee, even without any detailed fits to a specific model or the underlying accelerator populations.

For the primary CR "knee" at  $\sim 4 \times 10^{15}$  eV (Fowler et al. 2001; Antoni et al. 2005; Aartsen et al. 2013; Cao et al. 2024), the situation is still unclear, as observations from different experiments and using different techniques have unfortunately not yet fully converged, even at the very coarse level needed for the type of comparison we are seeking to make in this work. For example, early results presented in the Blümer et al. (2009) review, but also very recent results from the *Large High Altitude Air Shower Observatory* (LHAASO) experiment (Cao et al. 2024), indicate a small slope step (between 0.2 and 0.4), and the composition breaking *after* the spectrum. In the context of a simple fixed-rigidity source-cutoff knee described here, a slope step on the low side could be conceivably achieved with a combination of variations in both  $E_{p,max}$  and  $\gamma$  in the population of contributing sources. However, such a physical picture cannot accommodate the composition breaking after the spectrum. Even if we were to accept that, within uncertainties, composition and spectrum could be breaking together, this would point towards a population with very little spread in both  $\gamma$  and  $E_{p,max}$ , which would then result to a sharper slope step than the one observed. This combination of phenomenological observables then hint towards for a more complex picture – plausibly, for example, towards more than one source populations contributing cosmic rays around the primary knee, or additional physical effects (e.g., Hillas 1979). On the other hand, in the latest, post-LHC, reanalysis of data from the KASCADE-Grande experiment (Haungs et al. 2017; Chiavassa et al. 2019), the composition appears to be already getting heavier before the break in spectrum, while the slope step is reported at  $\sim 0.5$ , as might expected from the simplest version of fixed-rigidity knee explored here.

For the "second knee" around  $5 \times 10^{17}$  eV (see e.g. Bergman & Belz 2007 for a review), the observational situation is similarly unconverged. Different datasets disagree over the location of the composition break, and on whether, before the break, the composition was getting heavier (Cassiday et al. 1990) or lighter (HIRES/Mia Collaboration 2001; Abbasi et al. 2005). However there is consensus that the break is soft (slope step between 0.2 and 0.3), while the composition across the second knee is becoming *lighter*. Most likely then in this case there is a second, light (i.e., still efficiently accelerating) population contributing (e.g., Thoudam et al. 2016), so the simple physics we explored is not adequate to model this transition.

The knee-like "new feature" identified by the Pierre Auger Observatory in the cosmic ray spectrum around  $10^{19}$  eV (Aab et al. 2020) features a slope step of  $\sim 0.5$ , right in the expected range for a fixed-rigidity source-cutoff knee. This lends support to the interpretation that the break seen in composition-sensitive observables *before* the break in the spectrum Yushkov (2019b) indeed indicates a transition to heavier primaries. This is further reinforced by the reconstructed shape of the  $\langle \ln A \rangle$  spectrum. Although the overall normalization of the composition spectrum is very dependent on the choice for hadronic interaction modelling, the relative change of  $\langle \ln A \rangle$  with energy does feature the overall shape seen in the upper-right panel of Fig. 1:  $\langle \ln A \rangle$  flattens off between  $10^{18}$  and  $10^{18.5}$  eV, before starting to increase logarithmically around  $10^{18.6}$  eV. Our interpretation is then in overall agreement with the one proposed by Aab et al. (2020). Interestingly, however, the difference between the locations of the composition break (around  $10^{18.6}$  eV if we follow the same procedure we have used here to determine  $E_A$ ) and the spectrum break (reported by Aab et al. 2020 at  $10^{19.1}$  eV) is higher than the differences we have seen produced by variations in  $E_{p,max}$

alone. The implication is that  $\gamma$  may also be significantly varying in the dominant CR source population at these energies. This in turn could produce a non-negligible curvature in the spectrum before the break (see black dashed line in Fig. 4), that may be contributing to the curvature of the ankle, which is also located at the same energy as the composition break.

*Acknowledgements.* MF acknowledges support by the European Research Council under the European Union's Horizon 2020 research and innovation programme, grant agreement No. 771282 (PASIPHAE). VP acknowledges support by the Hellenic Foundation for Research and Innovation under the "First Call for H.F.R.I. Research Projects to support Faculty members and Researchers and the procurement of high-cost research equipment grant", Project 1552 CIRCE, and by the Foundation of Research and Technology - Hellas Synergy Grants Program (project MagMASim).

## References

- Aab, A., Abreu, P., Aglietta, M., et al. 2020, *Phys. Rev. D*, 102, 062005
- Aab, A., Abreu, P., Aglietta, M., et al. 2017, *J. Cosmology Astropart. Phys.*, 2017, 038
- Aartsen, M. G., Abbasi, R., Abdou, Y., et al. 2013, *Phys. Rev. D*, 88, 042004
- Abbasi, R. U., Abu-Zayyad, T., Archbold, G., et al. 2005, *ApJ*, 622, 910
- Amenomori, M., Ayabe, S., Bi, X. J., et al. 2008, *Nuclear Physics B Proceedings Supplements*, 175, 318
- Antoni, T., Apel, W. D., Badea, A. F., et al. 2005, *Astroparticle Physics*, 24, 1
- Bergman, D. R. & Belz, J. W. 2007, *Journal of Physics G Nuclear Physics*, 34, R359
- Bijay, B. & Bhadra, A. 2016, *Research in Astronomy and Astrophysics*, 16, 6
- Blümer, J., Engel, R., & Hörandel, J. R. 2009, *Progress in Particle and Nuclear Physics*, 63, 293
- Cao, Z., Aharonian, F., Axikegu, et al. 2024, *Phys. Rev. Lett.*, 132, 131002
- Cassiday, G. L., Cooper, R., Corbato, S. C., et al. 1990, *ApJ*, 356, 669
- Chiavassa, A., Apel, W. D., Arteaga-Velázquez, J. C., et al. 2019, in *European Physical Journal Web of Conferences*, Vol. 208, European Physical Journal Web of Conferences, 03002
- Deligny, O. 2020, arXiv e-prints, arXiv:2001.08811
- Diesing, R. 2023, arXiv e-prints, arXiv:2305.07697
- Ehlert, D., Oikonomou, F., & Unger, M. 2023, *Phys. Rev. D*, 107, 103045
- Fowler, J. W., Fortson, L. F., Jui, C. C. H., et al. 2001, *Astroparticle Physics*, 15, 49
- Guido, E., The Pierre Auger Collaboration, Abreu, P., et al. 2022, in *37th International Cosmic Ray Conference*, 311
- Haungs, A., Apel, W. D., Arteaga-Velázquez, J. C., et al. 2017, in *European Physical Journal Web of Conferences*, Vol. 145, European Physical Journal Web of Conferences, 13001
- Hillas, A. M. 1979, in *International Cosmic Ray Conference*, Vol. 8, International Cosmic Ray Conference, 7
- Hillas, A. M. 1984, *ARA&A*, 22, 425
- HIRES/Mia Collaboration. 2001, in *International Cosmic Ray Conference*, Vol. 1, International Cosmic Ray Conference, 374
- Hörandel, J. R. 2004, *Astroparticle Physics*, 21, 241
- Kimura, S. S., Murase, K., & Mészáros, P. 2018, *ApJ*, 866, 51
- Kotera, K. & Lemoine, M. 2008, *Phys. Rev. D*, 77, 023005
- Lemoine, M. 2005, *Phys. Rev. D*, 71, 083007
- Mollerach, S. & Roulet, E. 2019, *J. Cosmology Astropart. Phys.*, 2019, 017
- Mukhopadhyay, P., Peretti, E., Globus, N., Simeon, P., & Blandford, R. 2023, *ApJ*, 953, 49
- Muzio, M. S., Anchordoqui, L. A., & Unger, M. 2024, *Phys. Rev. D*, 109, 023006
- Nagano, M., Hara, T., Hatano, Y., et al. 1984, *Journal of Physics G Nuclear Physics*, 10, 1295
- Peters, B. 1961, *Il Nuovo Cimento (1955-1965)*, 22, 800
- Sanchez-Lucas, P. 2017, in *Proceedings of 35th International Cosmic Ray Conference — PoS(ICRC2017)*, Vol. 301, 495
- Sveshnikova, L. G. 2003, *A&A*, 409, 799
- Thoudam, S., Rachen, J. P., van Vliet, A., et al. 2016, *A&A*, 595, A33
- Workman, R. L., Burkert, V. D., Crede, V., et al. 2022, *Progress of Theoretical and Experimental Physics*, 2022, 083C01
- Yushkov, A. 2019a, in *International Cosmic Ray Conference*, Vol. 36, 36th International Cosmic Ray Conference (ICRC2019), 482
- Yushkov, A. 2019b, in *International Cosmic Ray Conference*, Vol. 36, 36th International Cosmic Ray Conference (ICRC2019), 482
- Yushkov, A., Bellido, J., Belz, J., et al. 2019, in *European Physical Journal Web of Conferences*, Vol. 210, European Physical Journal Web of Conferences, 01009
- Zhao, Y., Jia, H.-Y., & Zhu, F.-R. 2015, *Chinese Physics C*, 39, 125001